第 33 卷第 3 期
2017 年 3 月

无 机 化 学 学 报
CHINESE JOURNAL OF INORGANIC CHEMISTRY

Vol.33 No.3
501-508

氮化钛纳米管作为钒电池负极对V(Ⅱ)/V(Ⅲ)的电化学性能

赵峰鸣　闻　刚　孔丽瑶　褚有群　马淳安*
(浙江工业大学化学工程学院,绿色化学合成技术国家重点实验室培育基地,杭州　310032)

摘要：采用阳极氧化法在钛箔表面原位生长二氧化钛纳米管,随后在氨气氛围中氮化还原制备氮化钛纳米管,并将此电极直接作为钒电池的负极,研究其对 V(Ⅱ)/V(Ⅲ)的电化学性能。通过 X 射线衍射(XRD)、扫描电镜(SEM)以及 X 射线光电子能谱(XPS)等材料测试手段对氮化钛纳米管的形貌、组成和结构进行表征。分析结果表明,氨气高温氮化后,前驱体 TiO_2 相转变为 TiN 和 Ti_2N 相,表面元素组成为 Ti-N-O,Ti-N 和 Ti-O,且其形貌仍保持纳米管的微观结构。采用循环伏安,电化学阻抗和充放电测试表明,氮化钛纳米管对负极电解液中的 V(Ⅱ)/V(Ⅲ)展现了优异的电催化活性和可逆性，这主要归因于氮化钛纳米管大的电化学真实表面积和快速的电子转移通道。

关键词：氮化钛纳米管；钒电池；V(Ⅱ)/V(Ⅲ)；电化学性能
中图分类号：O646.5　　**文献标识码**：A　　**文章编号**：1001-4861(2017)03-0501-08
DOI:10.11862/CJIC.2017.053

Electrochemical Performance of Titanium Nitride Nanotubes as Negative Electrode in a Static Vanadium Battery Towards V(Ⅱ)/V(Ⅲ) Redox Couple

ZHAO Feng-Ming　WEN Gang　KONG Li-Yao　CHU You-Qun　MA Chun-An*
(*State Key Laboratory Breeding Base of Green Chemistry-Synthesis Technology, College of Chemical Engineering, Zhejiang University of Technology, Hangzhou*, 310032, *China*)

Abstract: In this study, titanium nitride nanotubes (TiN NTs) film is directly prepared on a Ti substrate through anodic oxidation process and subsequent nitridation in ammonia atmosphere. The prepared TiN NTs film is proposed as a novel catalyst towards V(Ⅱ)/V(Ⅲ) redox couple for the negative electrode in a static vanadium redox battery. Scanning electron microscopy (SEM) results confirm that TiN NTs retain its parental morphology of TiO_2 NTs. X-ray diffraction (XRD) pattern show that TiO_2 is transformed into TiN and Ti_2N. X-ray photoelectron spectroscopy (XPS) spectra reveal that the surface of TiN NTs is composed of Ti-N-O, Ti-N, Ti-O chemical states. Electrochemical properties of TiN NTs were characterized by cyclic voltammetry (CV) and electrochemical impedance spectroscopy (EIS). The higher peak current values and more symmetrical peak shape for V(Ⅱ)/V(Ⅲ) redox couple suggest the excellent electrochemical activity and reversibility of TiN NTs. EIS analysis revealed that the charge and mass transfer processes were accelerated at the TiN NTs electrode interface, which could be ascribed to the large electrochemical real surface area and fast transfer channel.

Keywords: titanium nitride nanotube; vanadium redox battery; V(Ⅱ)/V(Ⅲ); electrochemical performance

收稿日期:2016-10-17。收修改稿日期:2016-12-24。
浙江省自然科学基金(No.LY17B050006)资助项目。
*通信联系人。E-mail:science@zjut.edu.cn

0 Introduction

The vanadium redox battery (VRB) as a electrochemical energy conversion and storage device has recently attracted considerable attentions due to its outstanding advantages such as long cycle life, relatively large capacitance, high battery efficiency and environmental friendly[1-3]. In a VRB, V(Ⅳ)/V(Ⅴ) and V(Ⅱ)/V(Ⅲ) redox couples are used as positive and negative half cell, respectively, with the standard open circuit cell potential approximate 1.26 V[4]. The typical electrode materials for VRB are carbon materials such as carbon paper, graphite and carbon felt [5-7]. The advantages of these materials are their high porosity, large surface area and low electrical resistivity. However, the electrochemical reversibility of vanadium redox couples on the carbon materials is not good. Furthermore, the reaction kinetics of V(Ⅱ)/V(Ⅲ) redox couple is much slower than that of V(Ⅳ)/V(Ⅴ) redox couple on carbon electrodes[8]. The hydrogen evolution also happens easily on carbon electrodes in acid solution[9]. All of these effects limit the current efficiency and power density of VRB greatly. Considerable methods have been devoted to enhance the electrochemical activities of carbon materials, including thermal treatment[10], acid treatment[11], electrochemical oxidation[12], noble metal deposition[13], and modification of metal oxides such as TiO_2 [14], WO_3[15], Mn_3O_4[16]. The purpose of these methods is to introduce different functional groups to the carbon electrodes. Up to now, various methods have been used to improve the electrochemical performance of the positive electrode [17-19], but there are still limited reports to focus on the negative electrode or employ new materials[20].

Recently, titanium nitride (TiN) has received great attention because of its low electrical resistivity, high chemical stability and good corrosion resistance as well as extensive application in microelectronics industry, semiconductor industry and industrial machinery tools [21-24]. It is noted that TiN has shown noble metal-like behavior, due to the similarity of the electronic structure to that of the noble metals [25]. Thus, they can potentially be used in polymer electrolyte fuel cells[26], dye-sensitized solar cells[27], and electrochemical energy storage[28]. However, few works are found about TiN being used as an electrocatalyst in the VRB[29]. At present, most TiN nanomaterials have been prepared via a complex procedure by sputter-deposited coating with magnetron, laser or plasma[30-31]. The simple and direct nitridation of TiO_2 nanotubes (NTs) in an ammonia atmosphere is the effective way to obtain TiN NTs[32]. It is expected that the TiN NTs can be provided valid conductive network. The structure and conductive network of TiN NTs could accelerate the electron transport and improve the electrocatalytic performance for V(Ⅱ)/V(Ⅲ) redox couple.

The study aims to evaluate the effects of TiN NTs formed on Ti foil substrate and directly employed as a new negative electrode towards the performance of V(Ⅱ)/V(Ⅲ) redox couple in a static vanadium redox battery. The TiN NTs electrode was fabricated via a two-step process. These two steps involved the formation of TiO_2 NTs by anodization and a subsequent thermal nitridation. The charge-discharge measurement was conducted with a static battery under ambient conditions and the electrochemical performance of this negative electrode when used in VRB was studied.

1 Experimental

1.1 Materials and reagents

All the reagents and chemicals used were of analytical grade. Titanium foils with purity of 99.6% and thickness of 0.02 cm were purchased from Baoji Queen Titanium Co., Ltd. (China). Carbon felt with a thickness of 0.2 cm was obtained from Tieling Shenhe carbon fiber Co., Ltd (China). Graphite (DESAY, HT, SL) with a thickness of 0.2 cm was supplied by Wuxi Boou carbon industry Co., Ltd (China). $VOSO_4 \cdot xH_2O$ (99.9%) was purchased from shanghai Nuotai chemical factory (China). Nafion115 ion exchange membrane was obtained from Dupont (USA). High-purity NH_3 (99.999%) and N_2 (99.999%) were obtained from Hangzhou Minxin Gas Co., Ltd (China). HNO_3, H_2O_2

(30% , *V*/*V*, aqueous solution), NH_4F, $CO(NH_2)_2$, Na_2SO_4, NaF and H_2SO_4 (98%, *w*/*w*) were supplied by Shanghai Aladdin Chemical Reagent Company. All solutions and subsequent dilutions were prepared using deionized water.

1.2 Preparation and characterization

TiN NTs were fabricated via a two-step process. These two steps involved the formation of TiO_2 NTs by anodization and a subsequent thermal nitridation. In the first step, a Ti foil was pre-cut in coupons 3.0 cm ×3.0 cm. Prior to anodization, Ti foil was chemically polished in a mixed solution of 12.0 mL HNO_3+12.0 mL H_2O_2+5.0 g NH_4F+0.3 g $CO(NH_2)_2$ for 30 s until a mirror finish was exposed. The anodization was performed using a two-electrode cell with the Ti foil as the working electrode and a platinum foil as the counter electrode. The distance between Ti foil and the counter electrode was 2.0 cm. The nanotubes were formed in a mixed solution of 0.2 mol·L^{-1} Na_2SO_4 and 0.1 mol·L^{-1} NaF under a constant cell voltage of 20.0 V for 1.5 h. In the second step, the TiO_2 NTs prepared above was loaded into a silica tube reactor placed in a horizontal tubular furnace and connected to a gas feed system. Initially, a flow of nitrogen gas was maintained over the bed to remove all air and water for 30 min. Then the furnace was heated from room temperature to 450 ℃ at a rate of 20 ℃·min^{-1} and the film was annealed for 1 h. After the furnace temperature was sequentially heated from 450 to 850 ℃, the flowing gas was switched to NH_3 (160 mL·min^{-1}) and the nitriding reaction was carried out for 2 h. Finally, the TiN NTs were cooled via purging nitrogen gas.

The morphology of samples was determined by scanning electron microscopy (Hitachi S-4700) coupled with energy dispersive spectrometer (Thermo NORAN VANSTAGE ESI), using Cu *Kα* radiation. The crystalline structure was investigated by an X-ray Diffractometer (Rigakv D/max-III) using Cu *Kα* radiation. XPS measurements were carried out with a Kratos Axis Ultra DLD spectrometer (England), using a focused monochromatized Al *Kα* operated at 300 W. The base pressure was about 3×10^{-7} Pa. The binding energies were referenced to the C1*s* line at 284.6 eV from adventitious carbon.

1.3 Electrochemical measurements

CV behaviors were carried out using a CHI 660D instrument. The three-electrode cell consisted of a saturated calomel electrode (SCE) as the reference electrode, Pt foil as the counter electrode, and the TiO_2 NTs, TiN NTs, graphite with geometric area of 1.0 cm^2 as the working electrode, respectively. Potential steps experiments were carried out in 3.0 mol·L^{-1} H_2SO_4 solution. The EIS was measured by applying amplitude of 5 mV over the frequency ranging from 10^5 to 10^{-2} Hz. The potential was fixed at −0.6 V in all EIS measurements to ensure similar polarization. The electrolyte was 1.5 mol·L^{-1} V(Ⅲ)+ 3.0 mol·L^{-1} H_2SO_4 solution maintained by a water bath system at 25 ℃.

1.4 Charge-discharge test

The constant current charge and discharge test was carried out using a static vanadium redox battery. In a single cell structure, the conductive plastic plates were used as current collectors and Nafion 115 ion exchange membrane served as separator. The positive electrode was carbon felt (3 cm×3 cm×0.2 cm) and the negative electrode was TiN NTs (3 cm ×3 cm ×0.02 cm) or graphite (3 cm×3 cm×0.2 cm). Positive and negative electrolytes (1 mL in each half-cell) consisted of 1.5 mol·L^{-1} V(Ⅳ) and 1.5 mol·L^{-1} V(Ⅲ) in 3.0 mol·L^{-1} H_2SO_4 solution, respectively. The voltage range was fixed between 1.65 V and 0.8 V and the cell was charged and discharged at the current density of 5 mA·cm^{-2}.

2 Results and discussion

XRD pattern of TiN NTs is shown in Fig.1. Five peaks with a value of 2θ around 36.9°, 43.1°, 62.6°, 74.5° and 78.4° can be assigned to (111), (200), (220), (311) and (222) plants of TiN, respectively. The diffractogram of the sample shows peaks at 2θ around 39.2°, 40.8°, 51°, 61.1°, 64.2°, 67.3° and 73.2°, which are characteristics of Ti_2N. It indicates that the nanotube is composed of TiN and Ti_2N. No peaks of TiO_2 can be observed, which show that TiO_2 is

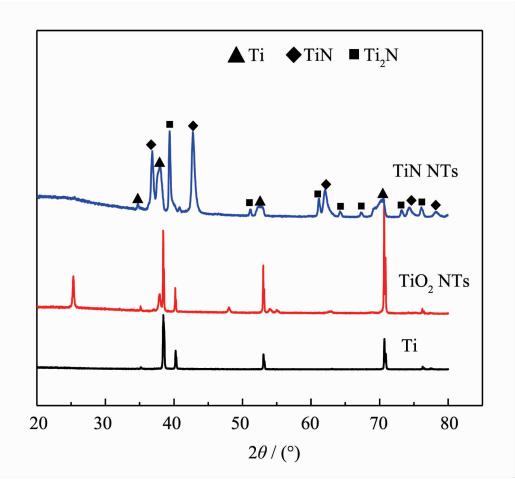


Fig.1 XRD patterns of Ti substrate, TiO_2 NTs and TiN NTs

transformed into TiN or Ti_2N.

XPS spectroscopy was further used to investigate the surface characterization and chemical states of TiN NTs (Fig.2). It is noticeable in the Ti2*p* spectra (Fig.2a) that multiple characteristic peaks are evolved into $Ti2p_{1/2}$ and $Ti2p_{3/2}$ regions. For $Ti2p_{1/2}$, the binding energies of the synthetic peaks at 461.3, 462.8 and 464.2 eV are consistent with the reported values for Ti-N, Ti-N-O and Ti-O bonds, respectively[33-34]. For $Ti2p_{3/2}$, the binding energies of the synthetic peaks at 455.8, 456.9 and 458.5 eV are also associated with Ti-N, Ti-N-O and Ti-O bonds, respectively[33-34]. The characteristic peaks collected from N1*s* region (Fig.2b) at binding energies of 397.2 and 396.2 eV are commonly assigned to Ti-N and Ti-N-O bonds[35-36]. A small peak at 398.6 eV might be ascribed to C-N bond. To summarize, the surface of the obtained TiN NTs exhibited a mixture of Ti-N-O, Ti-N and Ti-O chemical binding states.

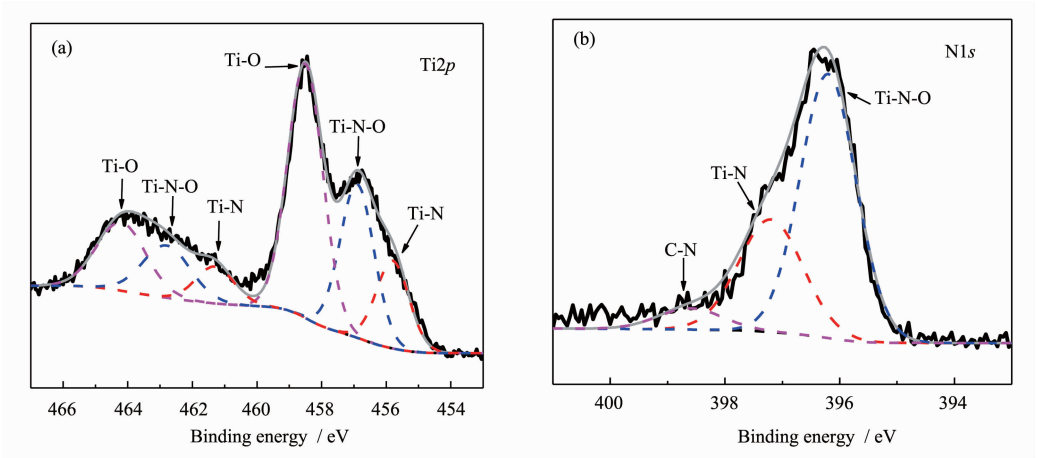


Fig.2 XPS spectra of (a) Ti2*p* and (b) N1*s* for TiN NTs

Fig.3 shows the morphologies of Ti substrate, TiO_2 NTs and TiN NTs, respectively. As shown in Fig. 3c, the obtained TiN NTs retains its parental morphology of TiO_2 NTs (Fig.3b). The nanotubes cannot be destroyed after calcinations at the high temperature in ammonia atmosphere. The hollow nanotubes of titanium nitride has an outer diameter of about 66~84 nm. The structure of nanotubes is advantageous for mass transfer of vanadium ions and can also provide a large surface area, which is confirmed by potential steps measurements.

The potential of electrodes was held at open

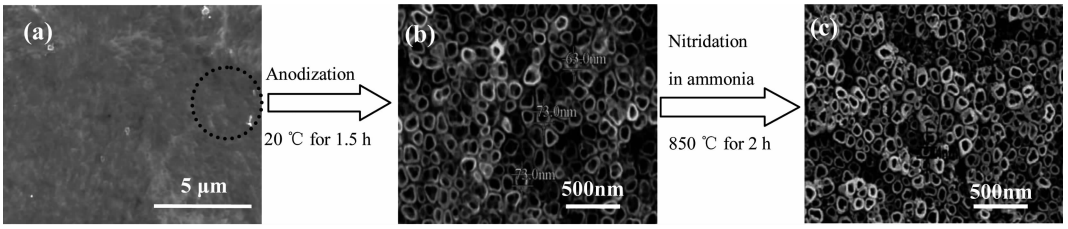


Fig.3 SEM images of (a) Ti substrate, (b) TiO_2 NTs, (c) TiN NTs

circuit potential versus SCE for 20 s, and then at the step amplitude of −0.1 V for 10 s. The roughness factor (ρ) was calculated according to the following equation[37]:

$$\rho = \frac{\int_0^t (i - i_\infty)dt}{\Delta\varphi C_N A_p} \quad (1)$$

In Eq.(1), i represents current, i_∞ represents stable current value after stepped and t is 10 s, $\Delta\varphi$ is 0.1 V, C_N is 20 μF·cm^{-2} and A_p represents the projected area of electrodes. The roughness factor (ρ) of polished Ti electrode, TiO_2 NTs electrode, TiN NTs electrode and graphite electrode are 87.62, 202.24, 1 014.88 and 244.34 cm^2·cm^{-2}, respectively. It is shown that the roughness factor (ρ) of the TiN NTs electrode is nearly 12 times as large as that of the polished Ti electrode, 5 times as large as the TiO_2 NTs electrode and 4 times as large as the graphite electrode, respectively. It indicates that anodic oxidation and subsequent nitridation is very useful to produce a larger electrochemical real surface area.

The CV behaviors of TiN NTs, TiO_2 NTs and graphite electrodes in 3.0 mol·L^{-1} H_2SO_4 solution are shown in Fig.4a. No obvious oxidation and reduction peaks appear except for the hydrogen evolution peak on the three electrode materials from −1.0 to 0 V (vs SCE). It is shown that the three electrodes are stable within the potential region in the H_2SO_4 solution. The TiN NTs electrode exhibits large double layer current density, indicating that the electrochemical active surface of TiN NTs is significantly large than that of TiO_2 NTs and graphite electrodes due to the large electrochemical surface real area of TiN NTs.

As illustrated in Fig.4b, CV behaviors of the three kinds of electrodes were investigated at scan rate of 50 mV·s^{-1} in the electrolyte containing 1.5 mol·L^{-1} V(Ⅲ)+3.0 mol·L^{-1} H_2SO_4 solution. The values of peak potential separation (ΔE_p) on the TiN NTs and graphite electrodes are 0.28 and 0.60 V, respectively. No obvious anodic and cathodic peaks are observed at the TiO_2 NTs electrode. The oxidation and reduction peak current of TiN NTs electrode is larger than that on the graphite electrode. This should be ascribed to the high electrical conductivity and more

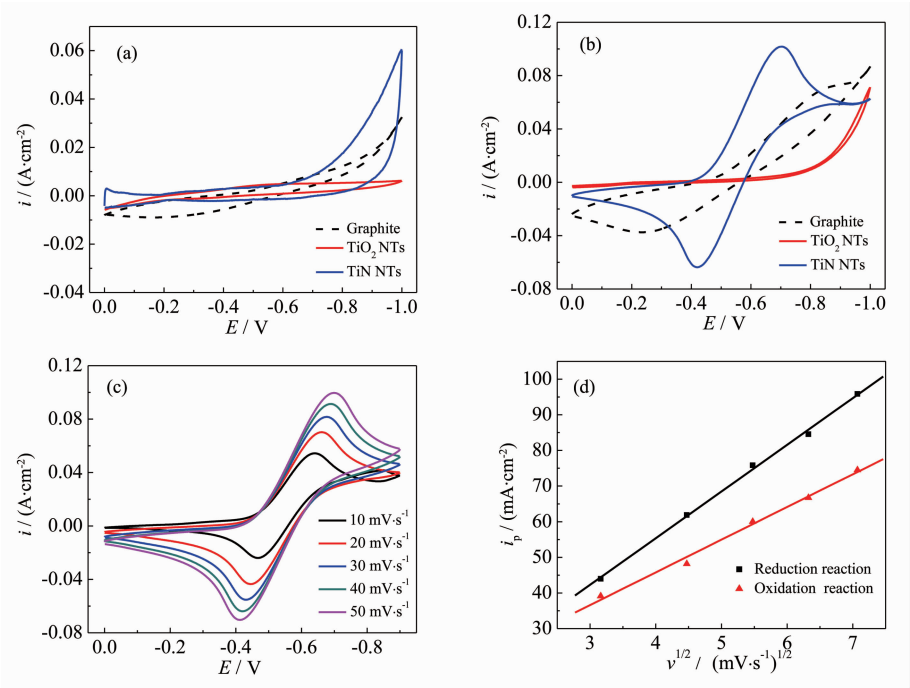


Fig.4　(a) CV curves of different electrodes in 3 mol·L^{-1} H_2SO_4 solution at the scan rate of 50 mV·s^{-1}; (b) CV curves taken on different electrodes in 1.5 mol·L^{-1} V(Ⅲ)+3.0 mol·L^{-1} H_2SO_4 solution at the scan rate of 50 mV·s^{-1}; (c) CV curves of TiN NTs electrode under different scan rates in 1.5 mol·L^{-1} V(Ⅲ)+3.0 mol·L^{-1} H_2SO_4 solution; (d) Variation peak current as a function of square root of the scan rate on the TiN NTs electrode

electrochemical active sites of TiN NTs electrode.

To further emphasize the above observation, CV behaviors of the TiN NTs electrode are recorded over a range of scan rates (Fig.4c). It shows that the peak potential separation and the values of i_{pa}/i_{pc} remain almost unchanged throughout the entire range of scan rates, which implies that the reversibility of the V(Ⅱ)/V(Ⅲ) redox reaction is far better for the electrode of TiN NTs than graphite electrode. According to the results of CV behaviors of different scan rates, the value of diffusion coefficient (D_o) for the quasi-reversible reaction can be evaluated by Eq.(**2**)[38]:

$$I_p = 2.69\times10^5 A n^{3/2} C_o D_o^{1/2} \nu^{1/2} \quad (2)$$

In Eq.(**2**), A is the area of the electrode (cm^2), n is the number of electron transfer, C_o is the bulk concentration of V(Ⅲ) ions ($mol\cdot L^{-1}$), ν is the scan rate ($mV\cdot s^{-1}$), I_p is the peak current (mA). Based on the known experimental conditions, Eq.(**2**) can be further transformed as follows:

$$D_o = 6.14\times10^{-6} k^2 \quad (3)$$

It is found that k refers to the slope of the line in point of the linear Eq.(**2**) and (**3**), where the variables are the reduction peak current density i_p and the square root of scan rate $\nu^{1/2}$. According to Fig.4d, the value of k is 13.10, thus the diffusion coefficient D_o for the cathodic reduction of V(Ⅲ) on the TiN NTs electrode is estimated to be 1.05×10^{-3} $cm^2\cdot s^{-1}$, which is about 10 times larger than that on the graphite electrode of 1.03×10^{-4} $cm^2\cdot s^{-1}$. It can be ascribed to the channels of 1D nanotubes on the surface of TiN NTs electrode, which the structure of nanotubes is helpful for mass and charge transfer of vanadium ions.

To better illustrate the relative enhancement of the catalytic activity of TiN NTs electrode, we have performed EIS measurements on the TiN NTs and graphite electrode, respectively. The obtained Nyquist plots are shown in Fig.5. It can be observed that the EIS of TiN NTs and graphite electrode both exhibit a typical semicircle at high frequency range and a straight line in the low frequency region. Based on the equivalent circuit (inset of Fig.5a), the charge-transfer resistance (R_{ct}) can be determined from the diameter of the leftmost semicircles, and the ohmic serial resistance (R_s) can be obtained by the intercept on the real axis at high frequency. Table 1 shows the R_s of the TiN NTs electrode were lower than that of the graphite electrode, due to the good electrical conductivity of TiN NTs electrode. The R_{ct} of TiN NTs and graphite electrodes are 0.25 and 4.90 $\Omega\cdot cm^2$. TiN NTs electrode has better electronic conductivity. This effect can be derived from the structure of TiN NTs electrode possesses a rapid charge-transfer process

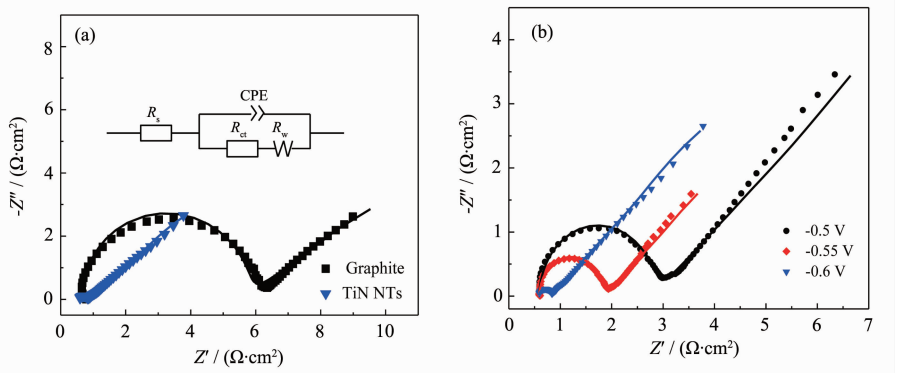


Fig.5 (a) Nyquist plots of different electrodes measured at a polarization potential of −0.6 V; (b) Nyquist plots of the TiN NTs electrode measured at various polarization potentials in the frequency range of 10^5 to 10^{-2} Hz.
Symbols: experimental data; lines: fitting curves

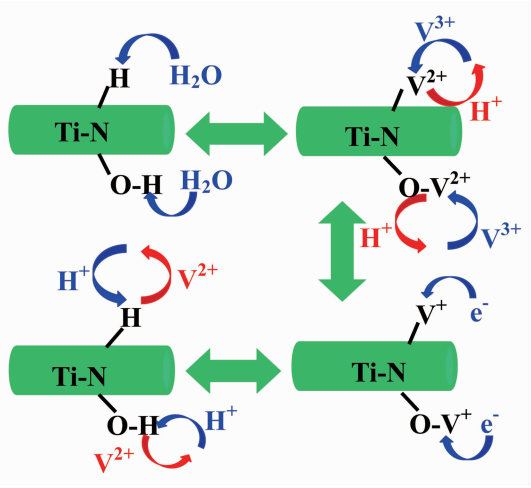
Table 1 Parameters obtained from the fitting curves of EIS

Electrode	R_s / ($\Omega\cdot cm^2$)	R_{ct} / ($\Omega\cdot cm^2$)	R_w / ($\Omega\cdot cm^2$)
Graphite	0.73	4.90	10.90
TiN NTs	0.58	0.25	5.92

and a fast mass transfer rate during the cathodic reduction process. Fig.5b shows that with the decreasing of the polarization potential, the R_{ct} is getting smaller as can be judged from the radius of the semicircle, which is correspond to the CV test results. This result can be attributed to the TiN NTs electrode has larger electrochemical surface area and more active sites for V(Ⅱ)/V(Ⅲ) redox couple.

The possible catalytic mechanism of V(Ⅱ)/V(Ⅲ) redox reaction at TiN NTs electrode was proposed according to the above experimental results. The detail reaction processes are shown in Scheme 1. In short, TiN NTs electrode provides large electrochemical surface area and more active center to improve the absorption of V(Ⅲ), therefore the TiN NTs electrode exhibited excellent electrochemical activity towards V(Ⅱ)/V(Ⅲ) redox couple.

Fig.6 displays the charge-discharge curves in a static VRB model with cutoff voltages of 0.8 and 1.65 V, respectively, at a current density of 5 mA · cm^{-2}. As is mentioned above that the V(Ⅱ)/V(Ⅲ) redox reaction can be accelerated on the TiN NTs electrode.



Scheme 1　Proposed mechanism on TiN NTs towards V(Ⅱ)/V(Ⅲ) redox reaction

As a result, the coulombic efficiency (CE), voltage efficiency (VE) and energy efficiency (EE) of the VRB system equipped with TiN NTs negative electrode can be enhanced (Fig.6a~c). By comparing the charge-discharge curves, the initial charge potential for the single cell of TiN NTs as negative electrode is lower and the onset discharge potential is higher than that of graphite as negative electrode (Fig.6d). Accordingly, it

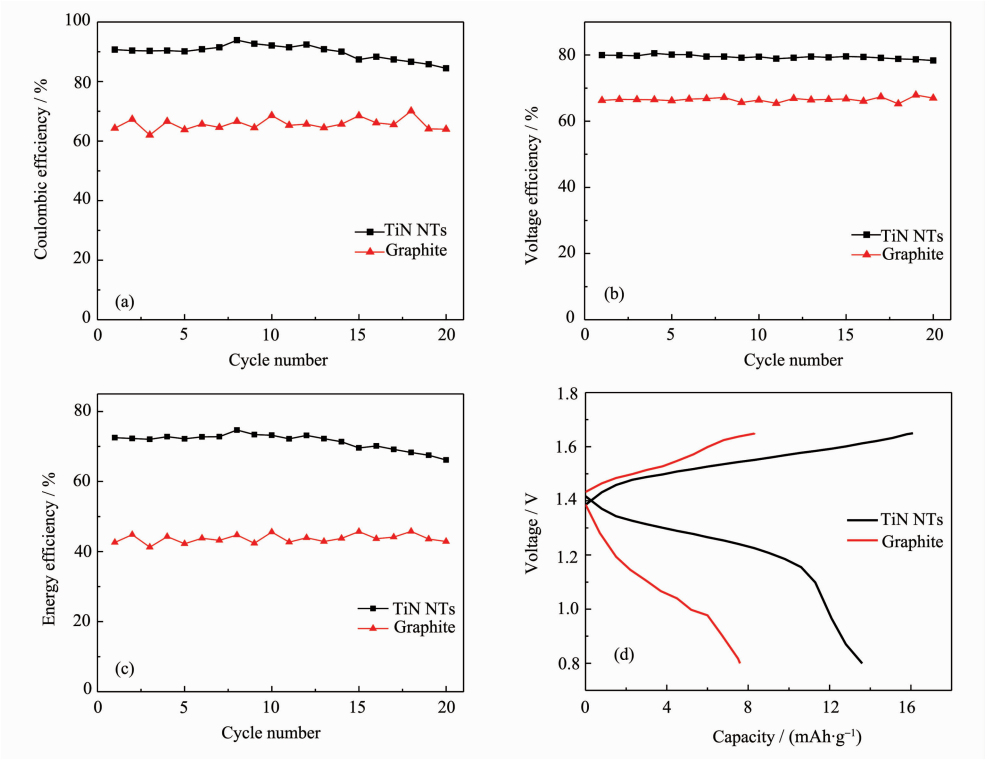


Fig.6　Performance comparison of battery with TiN NTs and graphite negative electrodes: (a) coulombic efficiency, (b) voltage efficiency, (c) energy efficiency and (d) charge and discharge curves

could be inferred that the TiN NTs could benefit to the V(Ⅱ)/V(Ⅲ) redox reaction by acting as a novel effective electrode catalyst for VRB. We think more effective methods of fabricating negative electrode, such as in situ growth of TiN NTs in foamed titanium or porous titanium should be studied in the future which will make the catalyst more stable during the flowing battery operation and enhance the battery performance.

3 Conclusions

In summary, TiN NTs has been successfully synthesized by anodization and subsequent nitridation on a Ti foil substrate. The nanotubes structure cannot be destroyed under ammonia reduction and nitridation. The TiN NTs film electrode for V(Ⅱ)/V(Ⅲ) has an excellent electrocatalytic performance due to its good conductivity, larger real contact area and more effective charge transport. It suggests that TiN NTs are promising alternative negative material in VRB.

References:

[1] Poullikkas A. *Renewable Sustainable Energ Rev.*, **2013**,**27**: 778-788

[2] Wang G, Chen J W, Wang X Q, et al. *J. Energy Chem.*, **2014**,**23**:73-81

[3] Parasuraman A, Lim T M, Menictas C, et al. *Electrochim. Acta*, **2013**,**101**:27-40

[4] Qian P, Zhang H M, Chen J, et al. *J. Power Source*, **2008**, **175**:613-620

[5] Mayrhuber I, Dennison C R, Kalra V, et al. *J. Power Sources*, **2014**,**260**:251-258

[6] Li B, Gu M, Nie Z M, et al. *Nano Lett.*, **2013**,**13**:1330-1335

[7] Yue L, Li W S, Sun F Q, et al. *Carbon*, **2010**,**48**:3079-3090

[8] Wei G L, Fan X Z, Liu J G, et al. *J. Power Sources*, **2015**, **281**:1-6

[9] Sun C N, Delnick F M, Baggetto L, et al. *J. Power Sources*, **2014**,**248**:560-564

[10]He Z X, Chen Z S, Meng W, et al. *J. Energy Chem.*, **2016**, **25**:720-726

[11]LIU Su-Qin(刘素琴), SHI Xiao-Hu(史小虎), HUANG Ke-Long(黄可龙), et al. *Chinese J. Inorg. Chem.* (无机化学学报), **2008**,**24**(7):1079-1083

[12]Men Y, Sun T. *Int. J. Electrochem. Sci.*, **2012**,**7**:3482-3488

[13]Wang W H, Wang X D. *Electrochim. Acta*, **2007**,**52**:6755-6762

[14]Tseng T M, Huang R H, Huang C Y, et al. *J. Electrochem. Soc.*, **2013**,**160**(8):A1269-A1275

[15]Yao C, Zhang H M, Liu T, et al. *J. Power Sources*, **2012**, **218**:455-461

[16]He Z X, Dai L, Liu S Q, et al. *Electrochim. Acta*, **2015**,**176**: 1434-1440

[17]Wu X X, Xu H F, Lu L. *J. Power Sources*, **2014**,**250**:274-278

[18]He Z X, He Y Y, Chen C, et al. *Ionics*, **2014**,**20**:949-955

[19]Liu H J, Xu Q, Yan C W, et al. *Electrochim. Acta*, **2011**,**56**: 8783-8790

[20]Shen J X, Liu S Q, He Z, et al. *Electrochim. Acta*, **2015**, **151**:297-305

[21]Kaskel S, Schlichte K, Kratzke T. *J. Mol. Catal. A-Chem.*, **2004**,**208**:291-298

[22]Lemme M C, Efavi J K, Mollenhauer T, et al. *Microelectron. Eng.*, **2006**,**83**:1551-1554

[23]Ponon N K, Appleby D J R, Arac E, et al. *Thin Solid Films*, **2015**,**578**:31-37

[24]Yazdani A, Soltanieh M, Aghajani H, et al. *Vacuum*, **2011**, **86**:131-139

[25]Ningthoujam R S, Gajbhiye N S. *Prog. Mater. Sci.*, **2015**,**70**: 50-154

[26]Kakinuma K, Wakasugi Y, Uchida M, et al. *Electrochim. Acta*, **2012**,**77**:279-284

[27]Wang G Q, Liu S M. *Mater. Lett.*, **2015**,**161**:294-296

[28]Xie Y B, Fang X Q. *Electrochim. Acta*, **2014**,**120**:273-283

[29]Yang C M, Wang H N, Lu S F, et al. *Electrochim. Acta*, **2015**,**182**:834-840

[30]Kumar K K, Raole P M, Rayjada P A, et al. *Surf. Coat. Technol.*, **2011**,**205**:S187-S191

[31]Yu H J, Tan T Y, Wu W, et al. *Curr. Appl. Phys.*, **2012**,**12**: 152-154

[32]Peng X, Huo K F, Fu J J, et al. *Chem. Commun.*, **2013**,**49**: 10172-10174

[33]Lu X H, Wang G M, Zhai T, et al. *Nano Lett.*, **2012**,**12**: 5376-5381

[34]Balogun M S, Yu M H, Li C, et al. *J. Mater. Chem. A*, **2014**, **2**:10825-10829

[35]Han Y J, Yue X, Jin Y S, et al. *J. Mater. Chem. A*, **2016**,4: 3673-3677

[36]Chan M H, Lu F H. *Thin Solid Films*, **2009**,**517**:5006-5009

[37]Zhao F M, Yan F, Qian Y, et al. *J. Electroanal. Chem.*, **2013**, **698**:31-38

[38]HUANG Fei(黄斐), WANG Gui-Xin(王贵欣), YAN Kang-Ping(闫康平), et al. *Chinese J. Inorg. Chem.* (无机化学学报), **2012**,**28**(5):898-904